POLITECNICO DI TORINO
Repository ISTITUZIONALE

Flexible and reusable parylene C mask technology for applications in cascade impactor air quality monitoring systems

Original
Flexible and reusable parylene C mask technology for applications in cascade impactor air quality monitoring systems / Vigna, L., Gottschalk, M., Cacocciola, N., Verna, A., Marasso, S.L., Seeger, S., Pirri, C.F., Cocuzza, M.. - In: MICRO AND NANO ENGINEERING. - ISSN 2590-0072. - ELETTRONICO. - 14:(2022), p. 100108. [10.1016/j.mne.2022.100108]

Availability:
This version is available at: 11583/2954012 since: 2022-01-28T14:33:47Z

Publisher:
Elsevier

Published
DOI:10.1016/j.mne.2022.100108

Terms of use:

This article is made available under terms and conditions as specified in the corresponding bibliographic description in the repository

Publisher copyright

(Article begins on next page)

13 October 2026

MNE 14 (2022) 100108

Contents lists available at ScienceDirect

Micro and Nano Engineering

journal homepage: www.sciencedirect.com/journal/micro-and-nano-engineering

Flexible and reusable parylene C mask technology for applications in cascade impactor air quality monitoring systems

L. Vigna [a], M. Gottschalk [b], N. Cacocciola [a], A. Verna [a], S.L. Marasso [a,c,*], S. Seeger [b], C.F. Pirri [a,d], M. Cocuzza [a,c]

[a] Dipartimento di Scienza Applicata e Tecnologia (DISAT), Politecnico di Torino, C.so Duca degli Abruzzi 24, 10129 Torino, Italy
[b] Bundesanstalt für Materialforschung und -prüfung (BAM), 12203 Berlin, Germany
[c] CNR-IMEM, Parco Area delle Scienze, 37a, 43124 Parma, Italy
[d] Istituto Italiano di Tecnologia, Center for Sustainable Future Technologies, Via Livorno 60, 10144 Torino, Italy

ARTICLE INFO

Keywords:
AEROMET II
Parylene C
Reference samples
Flexible shadow masks
Cascade impactor
Air quality monitoring
Micropatterning
Mask fabrication
Elemental aerosol analysis
TXRF

ABSTRACT

The development of traceable new methodologies to quantify elemental air pollutants in particulate matter (PM) supports modernization of methods used in air quality monitoring networks in Europe. In the framework of the EURAMET EMPIR AEROMET II project, the combination of cascade impactor aerosol sampling and total reflection X-ray fluorescence elemental spectroscopy (TXRF) was investigated. This technique requires a traceable calibration based on reference samples. This paper describes a new, simple and effective method to produce such reference samples using flexible, reusable, and low-cost parylene C shadow masks, fabricated by photolithographic steps. These shadow masks can be used to produce reference samples that mimic the Dekati cascade impactor's deposition patterns by applying as-prepared micro stencils to 30 mm acrylic substrates and evaporating a reference material (Ti) in arrangements of thin circular dots. The highly flexible direct patterning of acrylic discs with reference material, otherwise impossible with conventional photolithography, allows multiple reusing of the same micro stencils. The aspect ratios of the dots could be repeated with an error less than 4%. A first set of standard reference samples for the 13 stages of the Dekati cascade impactor was produced and preliminary TXRF measurements of the deposited Ti masses were performed. The centricity of the deposition patterns turned out to be an important parameter for the quality of the TXRF results. The parylene mask technology for the production of reference samples turns out to be a promising new approach for the traceable calibration of TXRF spectrometers for the quantification of element concentrations in environmental aerosol samples but, due to its great versatility, it could be used for several other micropatterning applications on conventional and unconventional substrates.

1. Introduction

Nowadays air pollution, that comes from both anthropogenic and natural sources, is the leading cause of environmentally related severe health effects related to cardiovascular and respiratory diseases and climate change concerns [1,2]. It is mainly caused by traffic, fossil fuel combustion, diesel automobiles exhaust, biomass burning and many industrial processes. Inhalable aerosol particles are the largest contributors. Generally, the smaller the size, the higher the toxicity due to their chemistry and volatility. Most of the times, particulate matter contains free radicals and inorganic pollutants like arsenic, nickel, lead, cadmium and mercury, which are among the air pollutants of interest within the European air quality guidelines. Alongside, a major contribution is given by several gaseous primary pollutants such as nitrogen oxides (NO_x), sulphur oxides (SO_x), ammonia (NH_3), carbon monoxide (CO), carbon dioxide (CO_2), methane (CH_4), chlorofluorocarbons (CFCs) and volatile organic compounds (VOCs). Breathing in polluted air may irritate our airways and can cause shortness of breath, wheezing, coughing, asthma episodes and chest pain. Asthma and lungs cancer seem to be exacerbated due to exposure to these fine particles, increasing the possibility of endanger human's health [3–5]. Many Italian cities, one above all Torino, have very high particulate matter (PM) concentrations, along with Warsaw, Sofia, Skopje and Sarajevo in Europe in 2021 [6]. Each year, if air pollution were reduced to acceptable levels, an estimate of

* Corresponding author at: Dipartimento di Scienza Applicata e Tecnologia (DISAT), Politecnico di Torino, C.so Duca degli Abruzzi 24, 10129 Torino, Italy.
E-mail address: simone.marasso@polito.it (S.L. Marasso).

https://doi.org/10.1016/j.mne.2022.100108
Received 19 November 2021; Received in revised form 17 January 2022; Accepted 22 January 2022
Available online 25 January 2022
2590-0072/© 2022 The Authors. Published by Elsevier B.V. This is an open access article under the CC BY-NC-ND license (http://creativecommons.org/licenses/by-nc-nd/4.0/).

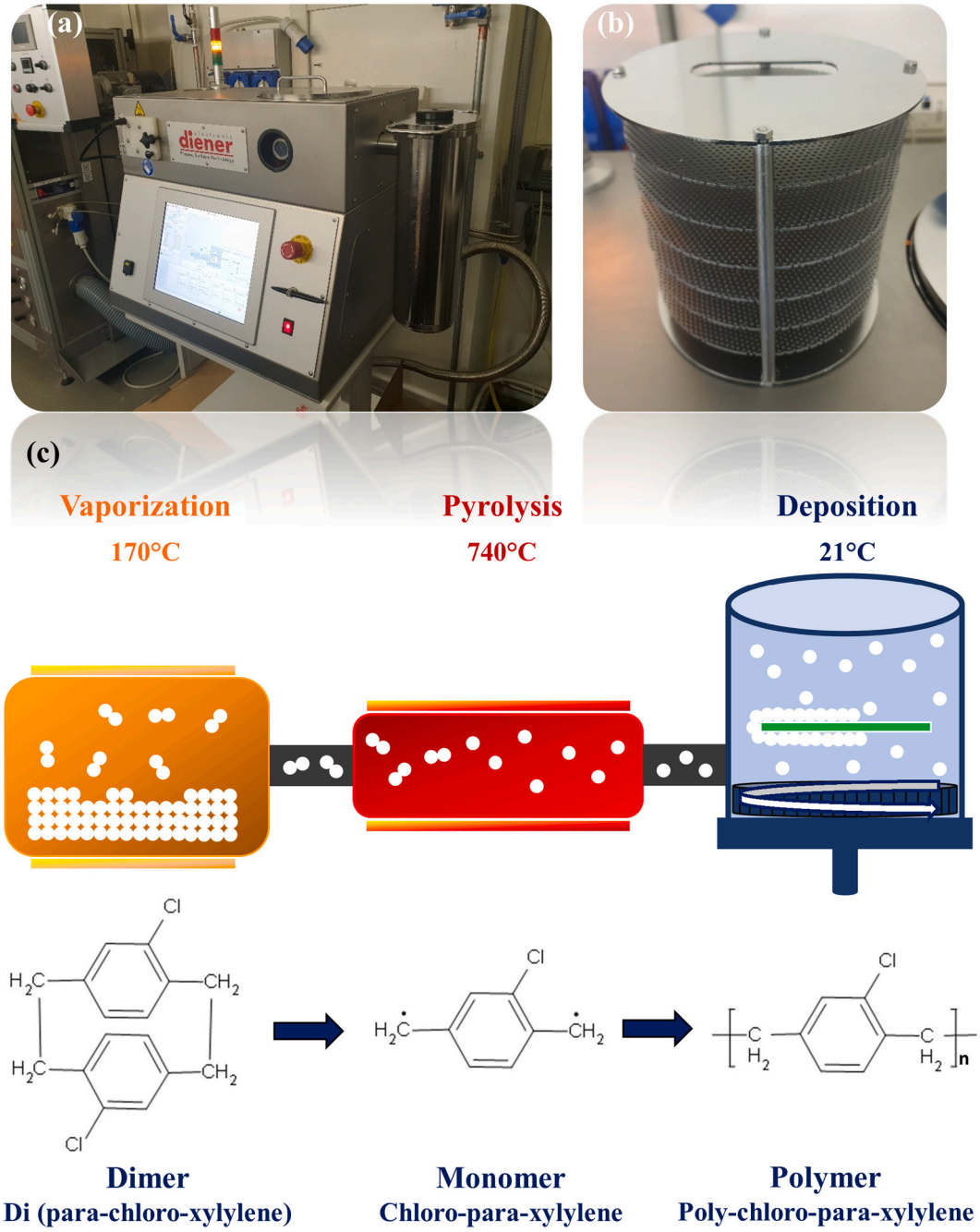

Fig. 1. (a) Diener Electronic – Parylene P6 deposition system (b) Multi-stage frame for samples loading into the deposition chamber (c) Sketch of the parylene C coating process, divided in three phases: the vaporization; the pyrolysis; and the deposition step. Beneath, the parylene C chemical formula from the dimeric powder to the deposited polymer.

4.2 million deaths could be avoided [7]. In order to actuate effective countermeasures against air pollution, air quality monitoring has to be improved. While the detection of pollutants in the gas form could be actuated in real-time by utilizing gas sensors with several different active materials [8–12], PM is usually collected over several days on filters, which have to be subsequently analyzed in the lab. Cascade impactors allow the size resolved collection of airborne PM and can be coupled with on-site semi-automated TXRF devices for the quantification of mass concentrations of the abovementioned elements with good time resolution and may supplement existing environmental monitoring nets. As any other analytical method of use, the combination of cascade impactor aerosol sampling with quantitative TXRF analysis requires traceable calibration. It is therefore of paramount importance to provide sets of standard reference materials which are as representative as possible to environmental aerosol samples.

Currently, in atmospheric research and air quality networks, there is a lack of traceable standards and harmonized calibration procedures for the elemental analysis of aerosols in terms of sensitivity and both time and spatial resolution [13]. Therefore, in the metrological framework, an important challenge that has to be tackled urgently is the development of certified standard reference substrates and traceable measurements techniques for the quantification of regulated and unregulated particulate air pollutants. In this way, it is possible to add value to the use of cascade impactor sampling coupled with TXRF spectroscopy for element mass concentration measurements in ambient air in an accurate way with fast response and low level of uncertainty [14]. This approach

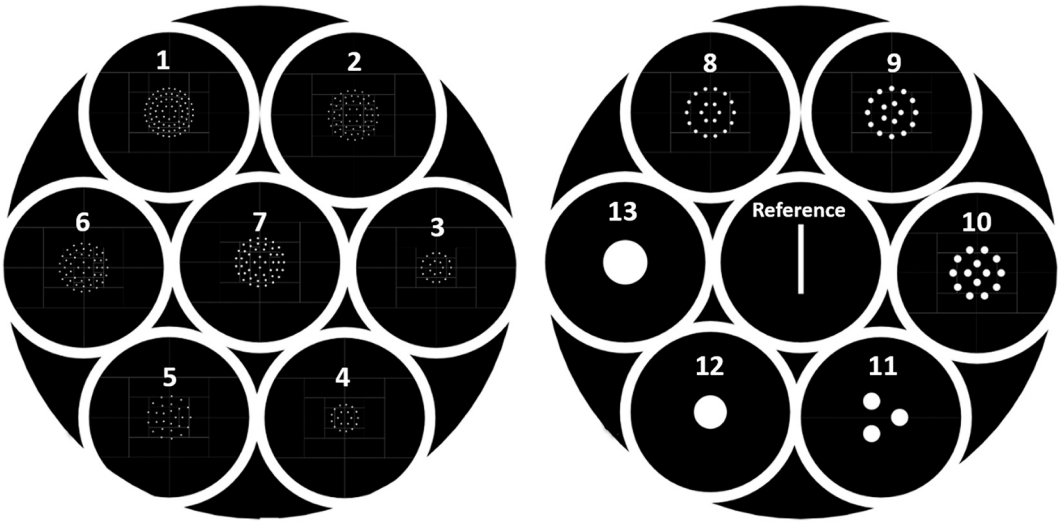

Fig. 2. Mylar masks with the negative image of the 13 stages of Dekati deposition patterns used for the photolithography.

was firstly introduced by Schneider in 1989 [15], but today there are several studies that are simplifying procedures of collecting samples and analyzing them on-site with portable technologies [13,14,16–18]. While TXRF spectrometers are calibratable against traceable and certified (multi-element) standards, which are prepared as centered, small point-like deposits on a sample carrier, there are no harmonized and standardized procedures available for the traceable analysis of cascade impactor samples with TXRF, were the deposits are spread over a carrier's surfaces.

For this reason, in the framework of EURAMET EMPIR AEROMET II project, the aim of this work is to design and produce a set of reference samples mimicking deposition patterns of cascade impactors such as the Dekati DLPI 10 on top of acrylic discs with the goal of containing the analyte under investigation in appropriate quantities with low tolerances in total mass and lateral distribution. In this paper, a new method, which is easily scalable to large-scale production, has been developed to obtain flexible, reusable, and low-cost parylene C shadow masks for cascade impactor air quality monitoring systems. Thanks to this micropatterning technique using shadow masks, important limitations are avoided, otherwise impossible with standard microfabrication processes. It can be performed on polymeric substrates without any solvent incompatibility and without high temperature treatments; due to the high flexibility, parylene C microstencils can be applied on topographically rough, non-planar and unconventional surfaces, impossible with rigid and expensive metallic shadow masks [19]. Furthermore, conventional microstencils made of metal or PDMS or SU-8 suffer of precise pattern high resolution due to the gap between the mask and the surface. The method proposed in this paper could solve these issues and it can be used for many purposes other than in the metrological field, from biomedical applications in the patterning of cells and proteins on different substrates [20–24] to the electronic fields for patterning organic transistors [21,25–27].

2. Experimental

2.1. Materials

The di-chloro-[2,2]-para-xylylene (Parylene C) was purchased from Diener Electronic (Ebhausen, Germany). Photolithographic steps were performed using AZ1518 (MicroChemicals, Germany) positive photoresist, AZ 400 K (MicroChemicals, Germany) developer, based on buffered KOH, and E6 etching solution (MicroChemicals, Germany) based on HNO_3, H_3PO_4 and acetic acid. Acetone (ACS reagent grade, $\geq$ 99.5%) and 2-propanol (IPA) (ACS reagent grade, $\geq$ 99.8%) were purchased from Sigma-Aldrich (Milano, Italy). All the chemicals were used as received without further purification. Deionized water (DI water) was obtained from a reverse osmosis (RO) purification system. Si 4″ wafers finished with a 1 μm thick thermally grown SiO_2 layer were purchased from Si-Mat (Kaufering, Germany) and used as a substrate for the shadow masks fabrication. Acrylic discs (30 mm diameter, 3 mm thickness) were gently provided by BAM.

2.2. Parylene C deposition

Parylene is a polymer which is obtained from the polymerization of para-xylylene ($H_2C{=}C_6H_4{=}CH_2$). The polymer has characteristics that make it interesting for use in electronic and medical fields, given its good properties as an electrical insulator, its hydrophobicity and its stability over time within biological tissues [28]. In this work, parylene C was deposited, a chlorinated variety of parylene obtained by replacing a hydrogen atom in the aryl ring with a chlorine atom. Parylene C is the most commonly used variety, given its low cost combined with its good electrical insulator characteristics [29]. In this work, the parylene deposition process was carried out with the Diener Electronic - Parylene P6 chemical vapor deposition (CVD) system (Fig. 1a). The coating process takes place at a pressure of 0.025 mbar and at a temperature of 30 °C and consists of three different phases all connected in one continuous vacuum stream, as shown in Fig. 1c. In the first one, the raw granular material, parylene-C dimer powder, is vaporized at a temperature of 170 °C, passing from the solid state to the dimeric gas form. The pyrolysis phase is then activated, in which the parylene gas is slowly diffused into a second chamber, where it undergoes a cleavage into monomers at a temperature of 740 °C. Finally, in the third phase, the monomer mixture is injected into the deposition chamber, where it is polymerized, molecule by molecule, on all surfaces of samples at room temperature as a thin, transparent polymeric layer. The samples are placed in a multi-stage frame (Fig. 1b), which is slowly rotated during the deposition process, to maintain the deposition as uniform as possible. Since it is applied as a vapor, the parylene C penetrates beneath, between, inside and around every component, avoiding edge effects, air gaps or voids, resulting in a uniform and complete deposition with optimal adhesion. The process stops when all the parylene loaded in the system is deposited in the chamber. For this reason, it is important to calibrate the quantity of parylene powder initially inserted in the loading door according to the desired thickness, taking into account the deposition rate which is (840 ± 120) nm/g. To prevent parylene from being deposited into the vacuum system during the deposition process, a liquid nitrogen cold trap is used. In our process an amount of parylene

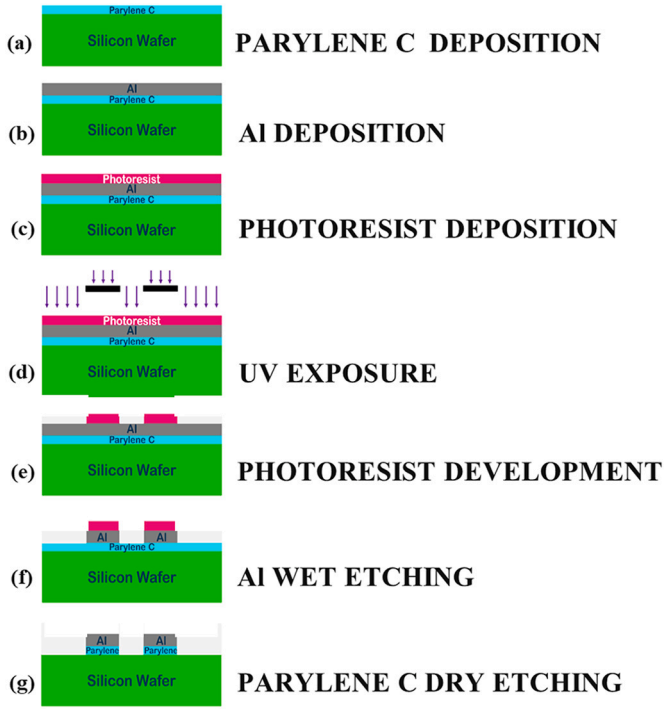

Fig. 3. Schematic representation of the parylene C microstencils fabrication process: (a) Parylene C deposition on top of the substrate, (b) Al thin film deposition; (c) Photoresist deposition; (d) UV exposure; (e) Photoresist development; (f) Al wet etching; (g) Parylene C dry etching.

equal to 7.5 g was used, resulting in a measured thickness of 7 μm.

In order to perform a micrometer-scaled selectively grown parylene structure with sharp features in one step approach during the deposition, it is also possible to treat the deposition silicon surface by evaporating certain transition metals like iron, metal salts and organometallic complexes that can be used to enhance the pattern process and act as inhibitors for the polymer's growth because it occurs only in the metal-free areas [30].

2.3. Technological steps details

Prior to the microstencils fabrication, two mylar masks (Fig. 2) were realized with the patterns of interest.

The shadow masks fabrication was implemented in a controlled clean room environment by using optical photolithographic steps as outlined in Fig. 3. A 4″, single side polished, P type, (100) Si wafer (resistivity 1–10 Ω·cm) finished with 1 μm thermal SiO_2 was used as substrate for the parylene C film deposition. The polymer films thickness was measured with a KLA Tencor P10 surface stylus profiler (California, U.S.A.). Multiple measurements were performed on the silicon wafer and the mean value was estimated. Then, a 100 nm thick film of Al was evaporated by means of an e-beam evaporator ($I = 60$ mA, rate = 4 Å/s) in order to be used as a hard mask for the successive parylene patterning. The desired layout of the Dekati stages were patterned by standard UV photolithography. AZ1518 positive photoresist was spin-coated and the wafer underwent a soft bake on a hotplate at 110 °C for 1 min. The substrate was selectively exposed under UV light for 7 s (10 mW/cm^2) through the mylar masks. Subsequently, the silicon wafer was developed in AZ 400 K diluted in deionized water with a 1:3 ratio and the exposed photoresist was removed. After the development, the Al hard mask is dissolved through a wet etching by using E6 solution, made of 5% HNO_3, 80% H_3PO_4 for etching the native aluminum oxide and acetic acid to improve the wettability as well as for buffering the solution to adjust the etching rate. At this point, dry etching was needed to create open parylene C areas by using a Vision 320 MK II reactive ion etcher (Plasma-Therm, U.S.A.) with an etching rate of 0.3 μm/min. After the dry etching, the remaining photoresist was eliminated through immersing the substrate in acetone first, and then rinsed in IPA and deionized water.

At this point, the photolithographic procedure is completed, and the shadow masks are ready to be used.

2.4. TXRF spectroscopy

In Total Reflection X-ray Fluorescence Spectroscopy (TXRF), an X-ray beam hits the surface of a sample below the critical angle, by which a total reflection of the beam on the surface occurs. Fig. 8 shows a schematic diagram for the spectrometer (TStar S4™, Bruker, Germany) used in this study. The fluorescence from the deposit contributes dominantly to the detected signal strength while the substrate signal is effectively attenuated. By this, deposited element masses of less than 1 ng can be detected [31]. A critical point in TXRF is the limited area of sample excitation by the X-ray beam and - by the detector aperture - limited fluorescence signal detection. These two factors may become important especially for depositions with large coverage, such as is the case for several stages of the Dekati impactor, and may cause systematic underestimation of the real deposited masses. Corrections to the TXRF raw data are required to compensate for this. Respective correction factors for each stage (i.e., for each deposition pattern) can be determined using reference samples with known quantities and typical deposition patterns. For the reasons mentioned above, off-centered laterally extended depositions could also falsify quantitative TXRF results and that is the reason why the centricity of the reference samples is a key quality parameter in the preparation process.

3. Results and discussion

In cascade impactors, disc-shaped carriers or substrates with smooth surfaces made of PMMA or quartz are used. Conventional methods for ambient aerosol analysis require stationary on-site filter sampling in combination with lab-based ion chromatography (IC), gravimetry, gas chromatography and mass spectroscopy (GC–MS) or inductively coupled plasma mass spectroscopy/optical emission spectrometry (ICP-MS/OES). They are not suitable for real-time particle size-resolved aerosol monitoring and the samples have to be stored and transported to a laboratory. The combination of cascade impactor sampling and portable TXRF on the other hand, provides a tool for a quick on-site and size-resolved analysis of aerosol samples. Short sampling times of several hours provide good time resolution. The method is non-destructive and allows for subsequent lab-based analytics. TXRF, as explained in the experimental section, is capable of detecting many elements in a concentration range down to typically 0.1 ng/m^3. The combination of cascade impactor sampling and TXRF needs traceable calibration in order to reliably quantify the mass concentration of elements of interest. This study describes the fabrication of a set of reference samples that mimic the deposition pattern of a particular commercial cascade impactor. Such sets of reference samples can be used to calibrate the whole method taking especially into account the affecting factors which come from the deposition patterns generated by the cascade impactor. The cascade impactor under investigation was the Dekati DLPI 10 (Dekati Ltd., Kangasala, Finland) low-pressure cascade impactor, characterized by 13 different stages with aerodynamic cut points of different sizes. Each stage has circular jets that generate a rotationally symmetric deposition pattern on the acrylic carriers (30 mm diameter, 3 mm thickness) [14]. Each pattern consists of small dots arranged in up to four concentric rings as shown in Fig. 2. With the procedure illustrated in the previous section, it was possible to realize the parylene C shadow masks on wafer. It is a very straightforward process that doesn't involve any particular difficulties. Acrylic discs were used as carriers. Using conventional photolithography, it's

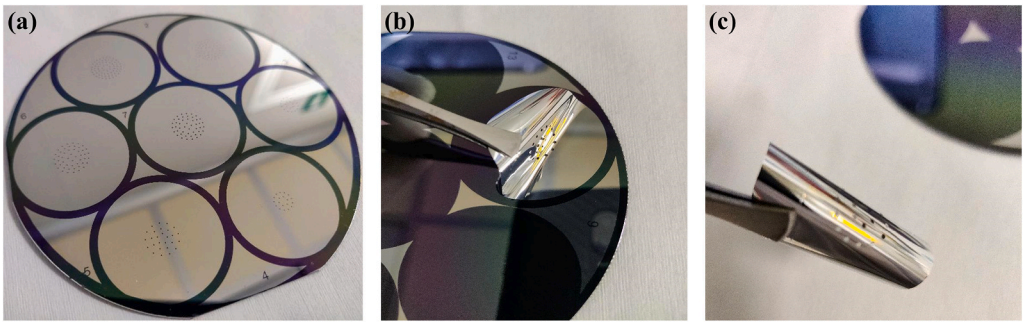

Fig. 4. Images of the peeling off process: (a) Single wafer with seven Parylene C shadow masks at the end of the fabrication process; (b) Single microstencil is lifted-off from the silicon wafer; (c) Flexible ready to use shadow mask.

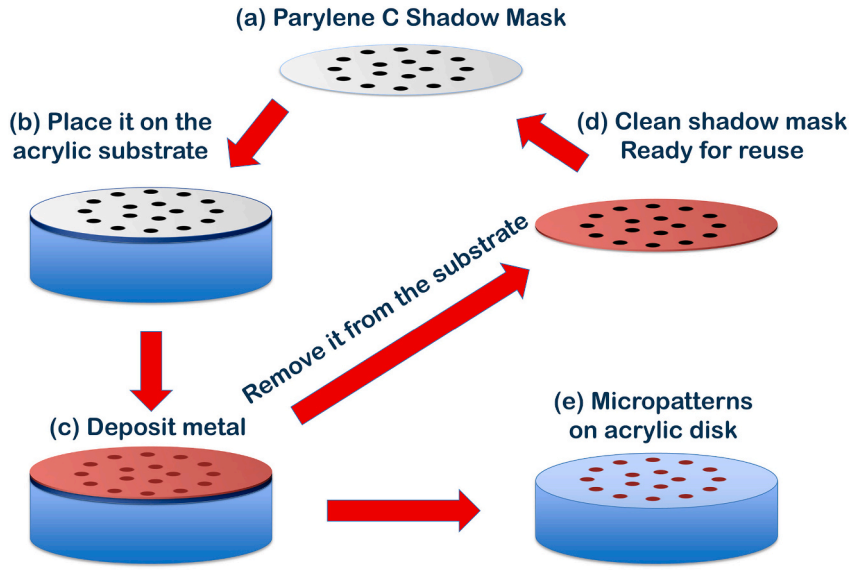

Fig. 5. Sketch of the steps required for the fabrication of a set of reference samples using parylene C shadow masks.

impossible to direct pattern on top of polymeric substrates. In fact, during the rinsing step to remove the excess of photoresist, the acetone would chemically attack the PMMA surface making it blurry. For solvent incompatibility, the standard process has to be discarded. Another issue that has been overcome is the carrier's thickness. Most of the mask aligners don't allow the use of thick substrates due to instruments design limitation. As shown in Fig. 4, the parylene C microstencils were easily peeled off one by one by using some tweezers and ready to be used. Up to the thickness of 7 μm, the patterned shadow masks are very flexible and reusable.

Fig. 5 illustrates the protocol followed for direct micropatterning the acrylic discs used as carriers in the cascade impactor utilizing the aforementioned fabricated parylene C shadow masks. By using this technology, there are no issues related to the use of incompatible solvents and, because of the flexibility and the microstencils easy handling, carrier's thickness is not a problem anymore.

Once the parylene C microstencil is peeled-off the silicon wafer, it is ready to use (Fig. 5a). In the first step, the shadow mask is applied on top of the acrylic disc where the pattern is needed (Fig. 5b). In the current implementation the alignment was manually performed by a skilled operator, nonetheless alternative more industrial-ready approaches can be easily applied (i.e., roll-to-roll, vacuum pick-and-place with a suitable holder, …). The parylene C membrane is quite thin and tends to fold on itself while being held with tweezers. On the contrary, there is an optimal adhesion between the substrate and the mask, avoiding any gap between them and any shift during the deposition. It was decided to use Ti as reference metal for the deposition step. 80 nm of Ti is deposited through an e-beam evaporator ($I = 120$ mA, rate = 5 Å/s) (Fig. 5c). Next, the microstencil is removed from the substrate, cleaned and ready to be reused after removing the deposited metal (Fig. 5d). At the end of the process, the acrylic disc is patterned with the Dekati layout, and it can be used as a standard reference sample (Fig. 5e). The obtained set of reference samples for air quality monitoring is shown in Fig. 6.

Fig. 7 shows the acrylic disc carrier's characterization performed with an optical microscope. Stage 3 carrier seems to be well realized. From the two top images, it can be depicted that the deposited Ti dots (yellow circles) are comparable in size and shape and hence the deposited mass is considerably the same in each dot. Several measurements were acquired on each sample for different dots and the mean values were estimated. The accuracy is good, and the pattern feature of stage 3 has an error of less than 4% (mostly due to the limited quality of the selected low-cost mylar mask-based patterning process) with a dot diameter of 288 μm instead of 300 μm.

In some preliminary TXRF experiments the TXRF peak intensities for Ti in the patterns of stages 4 and 11 were measured and compared, considering their orientation relative to the incoming X-ray beam in the TXRF spectrometer (Fig. 8). The deposition pattern of stage 11 is the largest of all patterns of the Dekati cascade impactor while the pattern of stage 4 has the smallest diameter. The patterns on stages 4 and 11 are both slightly off-center by approximately one millimeter. This lack of precision has - as we discuss below – an impact on the quantification with TXRF. The TXRF excitation energy was 17.4 keV (Mo-K_α), the

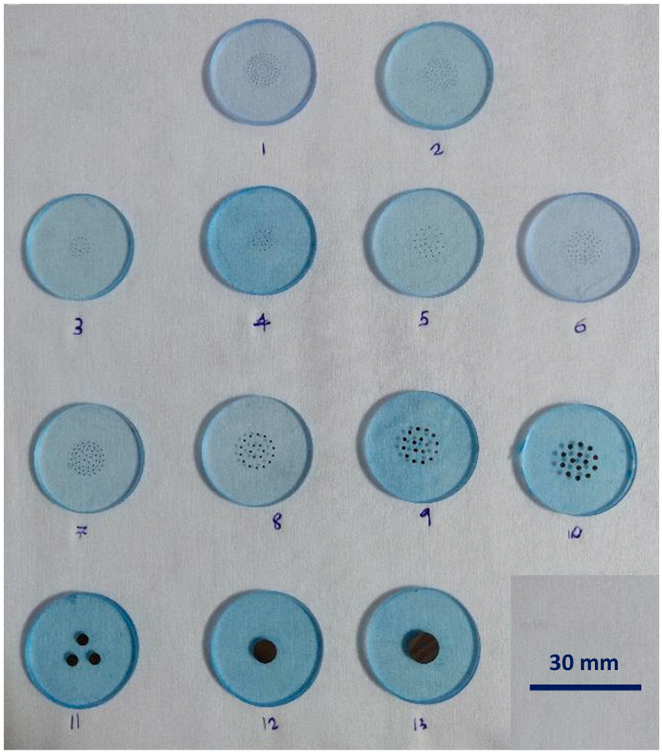

Fig. 6. Set of reference samples for cascade impactor air quality monitoring systems.

duration of the measurement was set to 300 live seconds and the angle of rotation was increased from 0° to 180° in steps of 30°. Each of the sample discs got an Edding permanent pen start marker for the rotation.

As can be seen on the right-hand side of Fig. 9, the stage 11 pattern has a circumscribing circle of approximately 10 mm in diameter, which is larger than the X-ray excitation area and also larger than the area of detection. In comparison, the diameter of the outer ring in stage 4 is 5 mm only and hence the deposit will be much more effectively excited, and the fluorescence radiation more effectively detected. The TXRF results are shown in Fig. 9 on the left side: for stage 4 the measured Ti peak intensities do practically not depend on the sample orientation, i.e., the angle of rotation, and show a standard deviation of only 1.5%. On the contrary, for stage 11 the Ti signal clearly depends on the angle of rotation.

Obviously, centricity becomes highly critical when the deposit pattern covers or even exceeds the excitation area. Two factors may become crucial in this case: a) the lateral excitation profile, which is non-circular and fades with distance to the center; and b) the radially decreasing detector efficiency which may additionally reduce the measured fluorescence intensity. The excitation of a not well centered deposit pattern as well as the detection of the fluorescence signal depend on the pattern orientation. Our results show that the effect is less critical if the deposit pattern is small and hence well illuminated by the incoming X-ray beam. In this case even a small eccentricity has obviously no drastic effect on the fluorescence signal. From our results we can identify the centricity of reference patterns as a quality parameter and a rough estimation of acceptable tolerances can be made which are clearly below 1 mm in xy-direction for circular patterns with diameters above 5 mm, e.g. for stage 11.

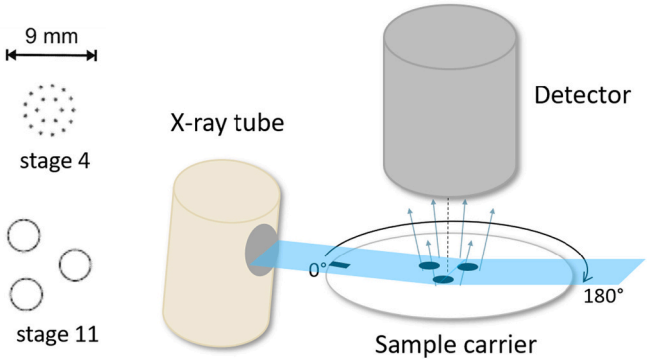

Fig. 8. On the left the patterns and dimensions of stages 4 and 11 are shown, while on the right a schematic of the TXRF spectrometer setup is reported with the arrow indicating the rotation of the sample.

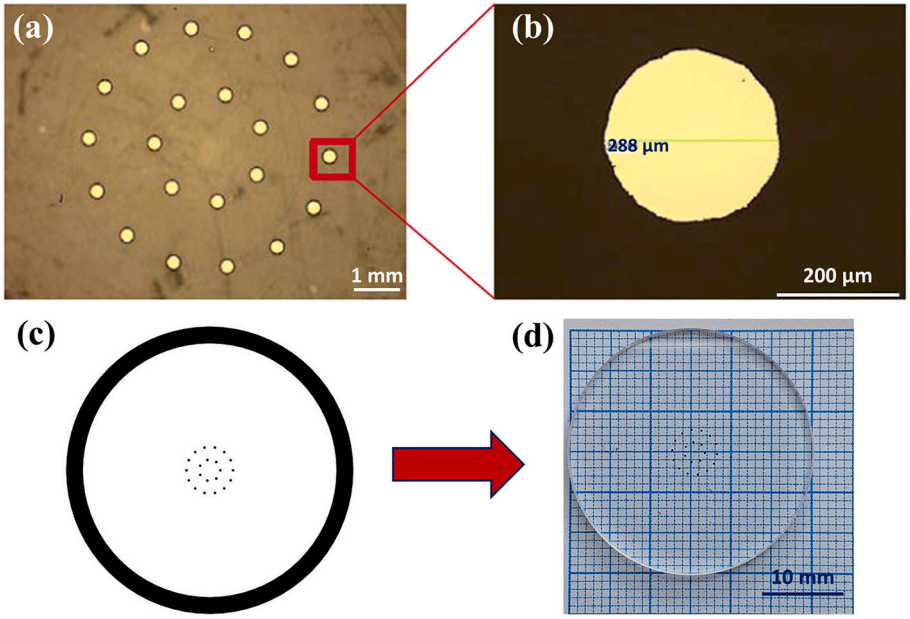

Fig. 7. (a) optical image of stage 3 reference sample (Ti dots in yellow and PMMA in brown); (b) enlargement of a single Ti dot; (c) stage 3 layout; (d) characterized Ti patterned acrylic disc stage 3 reference sample.

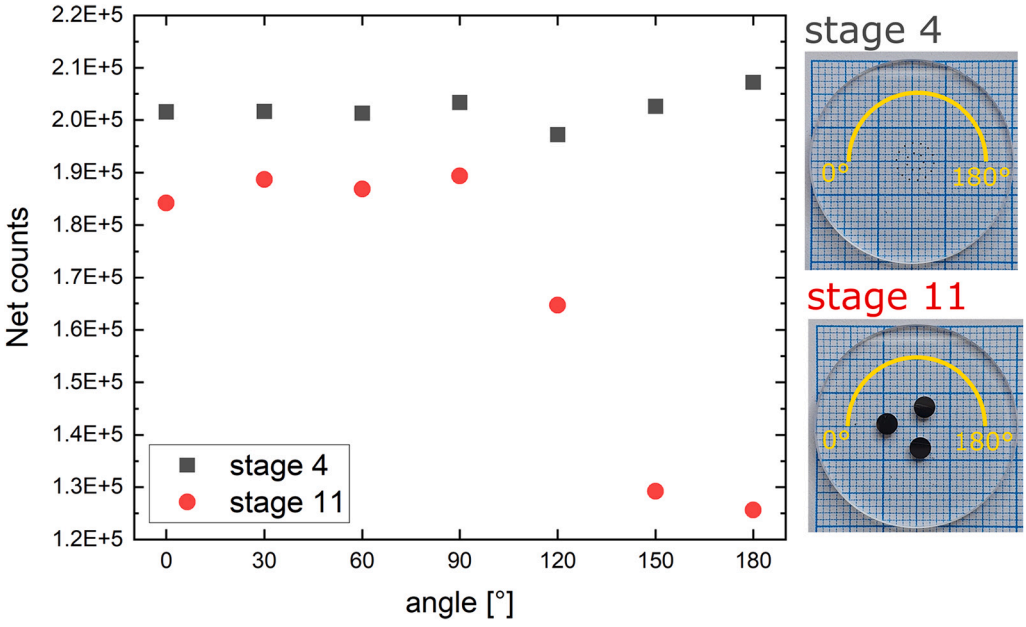

Fig. 9. Sample orientation dependency of the Ti net counts in stages 4 and 11.

4. Conclusions

In conclusion, this work illustrates a simple, accurate and effective method for the fabrication of parylene C shadow masks that can be utilized for realizing reference samples in the framework of air quality monitoring with cascade impactor sampling and TXRF spectroscopy. Highly flexible direct patterning of acrylic substrates otherwise impossible with conventional photolithography procedures was demonstrated, reproducing the cascade impactor patterns. Furthermore, parylene C microstencils were successfully reused multiple times without any damage or contamination. A very good accuracy was achieved on features down to 250 μm with an error in diameter less than 4%. This is a promising technology that can be scaled-up. The fabrication of sets of reference samples is an important step for the harmonized and traceable calibration of TXRF spectrometers and will enable them to become available to end users as commercial products, as well as providing much needed flexibility in the combination of elements in reference samples so that they can meet individual end user requirements. Motivated by the results, future work will focus on improving the centricity of patterns as one of the key quality parameters.

Funding

This work was supported by the EMPIR programme, co-financed by the Participating States and from the European Union's Horizon 2020 research and innovation programme, through grant agreement 19ENV08 AEROMET II.

CRediT authorship contribution statement

L. Vigna: Conceptualization, Data curation, Formal analysis, Investigation, Methodology, Validation, Visualization, Writing – original draft, Writing – review & editing. **M. Gottschalk:** Data curation, Investigation, Validation, Writing – original draft, Writing – review & editing. **N. Cacocciola:** Investigation, Writing – original draft, Writing – review & editing. **A. Verna:** Conceptualization, Formal analysis, Investigation, Methodology. **S.L. Marasso:** Conceptualization, Supervision, Writing – review & editing. **S. Seeger:** Conceptualization, Supervision, Writing – review & editing. **C.F. Pirri:** Funding acquisition. **M. Cocuzza:** Conceptualization, Supervision, Writing – review & editing.

Declaration of Competing Interest

The authors declare no conflict of interest. The funder had no role in the design of the study, in the collection, analysis, or interpretation of data, in the writing of the manuscript, or in the decision to publish the results.

References

[1] A.A. Almetwally, M. Bin-Jumah, A.A. Allam, Ambient air pollution and its influence on human health and welfare: an overview, Environ. Sci. Pollut. Res. 27 (2020) 24815–24830, https://doi.org/10.1007/s11356-020-09042-2.
[2] C.A. Pope, D.W. Dockery, Health effects of fine particulate air pollution: lines that connect, J. Air Waste Manage. Assoc. 56 (2006) 709–742, https://doi.org/10.1080/10473289.2006.10464485.
[3] M. Kampa, E. Castanas, Human health effects of air pollution, Environ. Pollut. 151 (2008) 362–367, https://doi.org/10.1016/j.envpol.2007.06.012.
[4] S. Fuzzi, U. Baltensperger, K. Carslaw, S. Decesari, H. Denier Van Der Gon, M. C. Facchini, D. Fowler, I. Koren, B. Langford, U. Lohmann, E. Nemitz, S. Pandis, I. Riipinen, Y. Rudich, M. Schaap, J.G. Slowik, D.V. Spracklen, E. Vignati, M. Wild, M. Williams, S. Gilardoni, Particulate matter, air quality and climate: lessons learned and future needs, Atmos. Chem. Phys. 15 (2015) 8217–8299, https://doi.org/10.5194/acp-15-8217-2015.
[5] E. Marino, M. Caruso, D. Campagna, R. Polosa, Impact of air quality on lung health: myth or reality? Ther. Adv. Chronic Dis. 6 (2015) 286–298, https://doi.org/10.1177/2040622315587256.
[6] European Environment Agency (EEA), Air Quality in Europe - 2020 Report. https://www.eea.europa.eu//publications/air-quality-in-europe-2020-report, 2020.
[7] WHO, WHO Global Air Quality Guidelines, 2021.
[8] L. Vigna, A. Fasoli, M. Cocuzza, F.C. Pirri, L.D. Bozano, M. Sangermano, A. Flexible, Highly sensitive, and selective chemiresistive gas sensor obtained by in situ photopolymerization of an acrylic resin in the presence of MWCNTs, Macromol. Mater. Eng. 1800453 (2018) 1800453, https://doi.org/10.1002/mame.201800453.
[9] L. Vigna, A. Verna, S.L. Marasso, M. Sangermano, P. D'Angelo, F.C. Pirri, M. Cocuzza, The effects of secondary doping on ink-jet printed PEDOT:PSS gas sensors for VOCs and NO2 detection, Sensors Actuators B Chem. 345 (2021), 130381, https://doi.org/10.1016/j.snb.2021.130381.
[10] L. Vigna, A. Nigro, A. Verna, I.V. Ferrari, S.L. Marasso, S. Bocchini, M. Fontana, A. Chiodoni, C.F. Pirri, M. Cocuzza, Layered double hydroxide-based gas sensors for VOC detection at room temperature, ACS Omega. 6 (2021) 20205–20217, https://doi.org/10.1021/acsomega.1c02038.
[11] P. Mishra, N.H. Tai, S.S. Islam Harsh, Transfer of microstructure pattern of CNTs onto flexible substrate using hot press technique for sensing applications, Mater. Res. Bull. 48 (2013) 2804–2808, https://doi.org/10.1016/j.materresbull.2013.04.021.

[12] J. Wu, Z. Wu, H. Ding, Y. Wei, W. Huang, X. Yang, Z. Li, L. Qiu, X. Wang, Flexible, 3D SnS2/reduced graphene oxide heterostructured NO2 sensor, Sensors Actuators B Chem. 305 (2020), 127445, https://doi.org/10.1016/j.snb.2019.127445.
[13] A. Bescond, C. Oster, P. Fisicaro, S. Goddard, P. Quincey, L.A. Tsakanika, T. Lymperopoulou, M. Ochsenkuehn-Petropoulou, Method for preparation of a candidate reference material of pm10 and pm2.5 airborne particulate filters loaded with incineration ash-inter comparison results for metal concentrations, Atmosphere (Basel). 12 (2021) 1–19, https://doi.org/10.3390/atmos12010067.
[14] S. Seeger, J. Osan, O. Czömpöly, A. Gross, H. Stosnach, L. Stabile, M. Ochsenkuehn-Petropoulou, L.A. Tsakanika, T. Lymperopoulou, S. Goddard, M. Fiebig, F. Gaie-Levrel, Y. Kayser, B. Beckhoff, Quantification of element mass concentrations in ambient aerosols by combination of cascade impactor sampling and mobile total reflection x-ray fluorescence spectroscopy, Atmosphere (Basel). 12 (2021), https://doi.org/10.3390/atmos12030309.
[15] B. Schneider, The determination of atmospheric trace metal concentrations by collection of aerosol particles on sample holders for total-reflection X-ray fluorescence, Spectrochim. Acta Part B At. Spectrosc. 44 (1989) 519–523, https://doi.org/10.1016/0584-8547(89)80059-X.
[16] Y. Kayser, J. Osán, P. Hönicke, B. Beckhoff, Peculiarities in Quantification of Airborne Particulate Matter by Means of Total Reflection X-ray Fluorescence, 2021, pp. 1–29. http://arxiv.org/abs/2101.09757.
[17] J. Osán, E. Börcsök, O. Czömpöly, C. Dian, V. Groma, L. Stabile, S. Török, Experimental evaluation of the in-the-field capabilities of total-reflection X-ray fluorescence analysis to trace fine and ultrafine aerosol particles in populated areas, Spectrochim. Acta - Part B At. Spectrosc. 167 (2020), https://doi.org/10.1016/j.sab.2020.105852.
[18] Y. Kayser, J. Osán, P. Hönicke, B. Beckhoff, Reliable compositional analysis of airborne particulate matter beyond the quantification limits of total reflection X-ray fluorescence, Anal. Chim. Acta 1192 (2021), 339367, https://doi.org/10.1016/j.aca.2021.339367.
[19] M. Graff, S.K. Mohanty, E. Moss, A.B. Frazier, Microstenciling: a generic technology for microscale patterning of vapor deposited materials, J. Microelectromech. Syst. 13 (2004) 956–962, https://doi.org/10.1109/JMEMS.2004.838368.
[20] I. Sanzari, M. Callisti, A. De Grazia, D.J. Evans, T. Polcar, T. Prodromakis, Parylene C topographic micropattern as a template for patterning PDMS and polyacrylamide hydrogel, Sci. Rep. 7 (2017) 1–11, https://doi.org/10.1038/s41598-017-05434-6.
[21] S. Selvarasah, S.H. Chao, C.L. Chen, S. Sridhar, A. Busnaina, A. Khademhosseini, M. R. Dokmeci, A reusable high aspect ratio parylene-C shadow mask technology for diverse micropatterning applications, Sensors Actuators A Phys. 145–146 (2008) 306–315, https://doi.org/10.1016/j.sna.2007.10.053.
[22] C.P. Tan, B.R. Cipriany, D.M. Lin, H.G. Craighead, Nanoscale resolution, multi-component biomolecular arrays generated by aligned printing with parylene peel-off, Nano Lett. 23 (2011) 1–7, https://doi.org/10.1021/nl903968s.Nanoscale.
[23] D. Wright, B. Rajalingam, J.M. Karp, S. Selvarasah, J. Yeh, R. Langer, M. R. Dokmeci, Reusable, reversibly sealable parylene membranes for cell and protein patterning, Biomed. Mater. Res. Part A. 85 (2010) 530–538, https://doi.org/10.1002/jbm.a.31281.Reusable.
[24] T. Trantidou, C. Rao, H. Barrett, P. Camelliti, K. Pinto, M.H. Yacoub, T. Athanasiou, C. Toumazou, C.M. Terracciano, T. Prodromakis, Selective hydrophilic modification of Parylene C films: a new approach to cell micro-patterning for synthetic biology applications, Biofabrication. 6 (2014), https://doi.org/10.1088/1758-5082/6/2/025004.
[25] J. Ortigoza-Diaz, K. Scholten, C. Larson, A. Cobo, T. Hudson, J. Yoo, A. Baldwin, A. W. Hirschberg, E. Meng, Techniques and considerations in the microfabrication of parylene c microelectromechanical systems, Micromachines. 9 (2018), https://doi.org/10.3390/mi9090422.
[26] H.W. Lo, W.C. Kuo, Y.J. Yang, Y.C. Tai, Recrystallized parylene as a mask for silicon chemical etching, in: 3rd IEEE Int. Conf. Nano/Micro Eng. Mol. Syst. NEMS, 2008, pp. 881–884, https://doi.org/10.1109/NEMS.2008.4484464.
[27] S. Zhang, E. Hubis, G. Tomasello, G. Soliveri, P. Kumar, F. Cicoira, Patterning of stretchable organic electrochemical transistors, Chem. Mater. 29 (2017) 3126–3132, https://doi.org/10.1021/acs.chemmater.7b00181.
[28] N. De La Oliva, M. Mueller, T. Stieglitz, X. Navarro, J. Del Valle, On the use of Parylene C polymer as substrate for peripheral nerve electrodes, Sci. Rep. 8 (2018) 1–12, https://doi.org/10.1038/s41598-018-24502-z.
[29] T. Marszalek, M. Gazicki-Lipman, J. Ulanski, Parylene C as a versatile dielectric material for organic field-effect transistors, Beilstein J. Nanotechnol. 8 (2017) 1532–1545, https://doi.org/10.3762/bjnano.8.155.
[30] K.M. Vaeth, K.F. Jensen, Transition metals for selective chemical vapor deposition of parylene-based polymers, Chem. Mater. 12 (2000) 1305–1313, https://doi.org/10.1021/cm990642p.
[31] B. Beckhoff, B. Kanngießer, N. Langhoff, R. Wedell, H. Wolff, Handbook of Practical X-Ray Fluorescence Analysis, Springer, Germany, 2006, https://doi.org/10.1007/978-3-540-36722-2.